Separation and Purification Technology 289 (2022) 120638

Contents lists available at ScienceDirect

Separation and Purification Technology

journal homepage: www.elsevier.com/locate/seppur

Eco-friendly mechanochemical synthesis of titania-graphene nanocomposites for pesticide photodegradation

Viviana Jehová González [a,*], Ester Vázquez [a,b], Beatriz Villajos [c], Alvaro Tolosana-Moranchel [d], Carlos Duran-Valle [e], Marisol Faraldos [c], Ana Bahamonde [c,*]

[a] Instituto Regional de Investigación Científica Aplicada (IRICA), UCLM, 13071 Ciudad Real, Spain
[b] Facultad de Ciencias y Tecnologías Químicas, UCLM, Avda. Camilo José Cela S/N, 13071, Ciudad Real, Spain
[c] Environmental Catalysis Engineering Group, Instituto de Catálisis y Petroleoquímica, ICP-CSIC, Marie Curie 2, 28049 Madrid, Spain
[d] Nanotechnology and Integrated BioEngineering Centre, School of Engineering, Ulster University, Northern Ireland, BT37 0QB, United Kingdom
[e] IACYS, Universidad de Extremadura, Av. Elvas S/N, 06006 Badajoz Spain

ARTICLE INFO

Keywords:
Graphene
TiO_2
Nanoparticles
Environmental
Pesticides

ABSTRACT

Titania graphene hybrid nanocomposites (TiO_2-FLG) synthesized from graphite and TiO_2 precursors, in a simple and sustainable approach via a three-step method, including the mechanochemical treatment of pre-synthesized FLG and TiO_2 NPs are efficient has led to the preparation of TiO_2-FLG as efficient nano-catalysts for photocatalytic degradation of a complex mixing of pesticides (isoproturon, pyrimethanil, alachlor and methomyl). The effect of few layer graphene (FLG) loading (0–1.0%) was analyzed to define the optimal ratio of FLG to TiO_2 and compared with the corresponding physical mixtures. X-ray Powder Diffraction (XRD) patterns of all these hybrid photocatalysts have presented the same crystal structure, with anatase as the main crystalline phase and brookite as secondary phase. An interaction between the graphene structure and the TiO_2 nanoparticles has been observed from Energy Dispersive X-Ray (EDX), X-ray photoelectron (XPS) and Raman spectroscopy studies, indicating that FLG is mainly deposited on the surface wrapping the TiO_2 nanoparticles. The presence of FLG in low concentrations and the mechanochemical activation are the key steps to improve the photocatalytic activity of TiO_2 nanoparticles on these hybrid nanocomposites. The TiO_2-FLG-0.5% hybrid nanocomposite, with circa 1.9 % content of graphitic carbon in surface, has showed the best photocatalytic performance in the degradation of pesticides. Pesticides were completely removed at 350 min, and around 82 % of total organic carbon (TOC) conversion was achieved at 540 min of irradiation time.

1. Introduction

Pesticide use is still increasing, mainly due to their use in the agricultural sector1 to both control pests for public health and for product storage-related applications. The mixing of otherwise clean bodies of water with water used for irrigation in fields also leads to contamination as the latter is likely to contain large amounts of fertilizers, pesticides, and herbicides, several of which have negative effects on humans and animals when consumed. In this context, one principal disadvantage of these chemical compounds is their toxic accumulation as persistent organic pollutants (POPs) in water and in the environment as a result of leakage into groundwater, soil and their ability to volatilize [1–4] As such, the development of efficient technologies for removing these POPs from environmental resources, including water, is currently still a major concern [5]. There are many different treatments for removing toxic pollutants from water and wastewater, including the application of advanced oxidation processes (AOPs) [6], which provide a viable and effective attenuation option for purifying wastewater contaminated

Abbreviations: TiO_2-FLG, Titania graphene hybrid nanocomposites; FLG, Few layer graphene; XRD, X-ray Powder Diffraction; EDX, Energy Dispersive X-Ray; XPS, X-ray photoelectron; TOC, Total organic carbon; POPs, Persistent organic pollutants; AOPs, Advanced oxidation processes; GO, Graphene oxide; rGO, Reduced graphene oxide; TGA, Thermogravimetric analyses; TEM, Transmission Electron Microscopy; HRTEM, High-Resolution Transmission Electron Microscope; SEM, Scanning Electron Microscopy; EDS, Energy Dispersive Spectroscopy; EBSD, Electron Backscatter Diffraction; HPLC, High-Pressure Liquid Chromatography; L-H, Langmuir-Hinshelwood.

* Corresponding authors.
E-mail addresses: vivianaj.gonzalez@uclm.es (V.J. González), abahamonde@icp.csic.es (A. Bahamonde).

https://doi.org/10.1016/j.seppur.2022.120638
Received 25 October 2021; Received in revised form 3 February 2022; Accepted 5 February 2022
Available online 8 February 2022

with POPs as they can be managed to oxidize a wide range of organic chemicals with excellent removal efficiency [7,8]. Photocatalysis is currently one of the most promising approaches for transforming recalcitrant pollutants into harmless substances [9] in an environmentally friendly way due to its low production costs, rapid degradation of pollutants without the generation of sludge, strong oxidizing power under ultraviolet irradiation [5], and the possibility of being applied in aqueous environments by utilizing solar energy [10–13].

One of the most attractive and efficient semiconductor photocatalyst is TiO_2 [14]. However, despite its high versatility, TiO_2 presents some significant disadvantages[15]; for that reason, many strategies are being developed to improve its photocatalytic performance (enhancing the visible light absorption and through the reduction of fast electron–hole recombination) including doping with non-metallic particles, noble metals or transition metal elements [16–18], adding an adsorbent [19,20], and through the heterojunctions with other nanomaterials, such as graphene, [16] to improve the separation between free carriers [21–28]. In fact, due to their interesting properties, various 2D nanomaterials have been used in the treatment and degradation of pesticides demonstrating promising results in this area, with high efficiency compared to conventional technologies [29].

Graphene is a one-atom-thick monolayer of carbon atoms packed in a two-dimensional honeycomb lattice, which has interesting physical, chemical, electronic, thermal, and mechanical properties[30], high charge carrier mobility[31–33], specific surface area ($\sim 2600\ m^2\ g^{-1}$) [32], and adsorption capacity All these excellent properties make graphene a good candidate in applications in solar cells and photoactive catalysts[34], being an excellent material in the synthesis of new hybrid structures to improve the performance of TiO_2 base photocatalysts [29,35–38].

Different strategies are currently being implemented to achieve new optimized titanium-graphene nanocomposites. On the one hand, by means of new safer, more ecological and less waste-generating graphene syntheses using natural or biocompatible reducing agents; and, on the other hand, to improve the interaction and formation of Ti—C and/or Ti—O—C bonds between TiO_2 and graphene, thus achieving a good hybrid graphene-TiO_2 photocatalyst. In order to improve this interaction, new developments have been designed in recent years that use different organic molecules or polymers to functionalize graphene and facilitate the anchoring of TiO_2 nanoparticles, leading to more efficient and durable photocatalyst composites[39,40].

Herein, a process for preparing few-layer graphene (FLG) by exfoliation of graphite, with melamine as exfoliating agent in a mechanochemical treatment, according to a previously published protocol [41,42] is used to obtain the starting graphene material directly. The novelty of this work lies in the development of a procedure for the synthesis of TiO_2-FLG hybrid nanocomposites based on the union of titanium oxide directly with graphene by means of mechanochemical synthesis. Unlike other syntheses of this type of hybrid photocatalyst, in which a previous step involving graphene oxide (GO) or even reduced graphene oxide (rGO) is required, in this case the graphite oxidation step to produce GO was omitted, thereby avoiding the use of large quantities of corrosive and polluting reagents.

In this context, the main goal of this work consisted in optimizing a synthetic methodology to obtain hybrid TiO_2-FLG nanocomposites for application in the photocatalytic degradation of relevant concentrations of a complex mix of pesticides classified by EU as priority pollutants (isoproturon, alachlor, methomyl and pyrimethanil). These pesticides are included in the European Water Framework Directive 2013/39/EU and in the Watch List of Decision 2015/495/EU [43]. The effect of FLG loading in the hybrid photocatalysts was analyzed to define an optimal ratio of FLG to TiO_2 and compared to physical mixtures of TiO_2 + FLG to discriminate the existence of a synergic effect in the photocatalytic process studied.

2. Material and methods

2.1. Photocatalysts synthesis

2.1.1. Mechanochemical production of Few-Layer graphene (FLG).

FLG was synthesized by exfoliation of graphite using melamine as exfoliating agent through a green mechanochemical treatment as previously published protocol.[41] FLG was prepared by mechanochemical treatment [41] using graphite (7.5 mg SP-1 graphite powder, purchased from Bay Carbon, Inc.) as the material precursor and melamine (22.5 mg Sigma Aldrich ref. M2659) as exfoliating agent. Both materials were milled in a Retsch PM 100 planetary mill at 100 rpm for 30 min, in a 25 mL stainless steel jar with ten stainless steel balls with 1 cm in diameter each. Therefore, the resultant solid was dispersed in 20 mL of water for further dialyzation at 70 °C. Finally, after five days of sedimentation, the supernatant was extracted to collect the resultant graphene dispersion. Powder graphene was obtained by lyophilizing the final dispersion (−80 °C at a pressure of 0.005 bar).

2.1.2. Synthesis of TiO_2 nanoparticles.

In an Erlenmeyer, 100 mL of Ethanol and 400 μL of KCl (0.01 M−pH 8.5) were added with stirring at 1200 rpm, after that 4.4 mL of Ti precursor (titanium isopropoxide) were poured. When a white precipitation was observed the stirring was decreased at 150 rpm (approx. 1 min) for 6 h and the Erlenmeyer was covered by Parafilm®, followed for further dialysis (7 changes each 2 h). After that, the TiO_2 was lyophilized for 2 days at −80 °C at a pressure of 0.005 bar.

2.1.3. Mechanochemical synthesis of few layer graphene (FLG) decorated with TiO_2 nanoparticles- hybrid nanocomposites.

All hybrid photocatalysts were prepared as following: FLG was mixed with pre-synthesized TiO_2 NPs with a proportion of FLG from 0.1 to 1 wt % in a Retsch PM100 planetary mill at 30 min and 100 rpm in zirconium grinding bowl of 250 mL with 15 zirconium balls (1 cm diameter) in air atmosphere. The resulting solid mixtures were dispersed in 100 mL water for further lyophilization for 72 h at −80 °C and pressure of 0.005 bar. The hybrid nanocomposites are nominated as TiO_2-FLG X %, where X corresponds to FLG percentage added in the synthesis procedure, in wt. %.

2.1.4. Physical mixtures of few layer graphene plus TiO_2 nanoparticles

Two different photocatalysts based on physical mixtures of FLG and TiO_2 nanoparticles have been prepared through mortar and sonication of both materials.

TiO_2 + FLG 0.5 %-sonicated catalyst was obtained by mixing 300 mg TiO_2 NPs, 1.5 mg FLG, and 100 mL of water. This solution was ultrasonicated during 30 min, following by lyophilization at the same conditions explained above.

Finally, 1.5 mg of FLG and 300 mg of TiO_2 nanoparticles were mixed manually in an agate mortar (80 mm in diameter and 30 mL) with pestle for 30 min. After this treatment, the obtained powder was dispersed in 100 mL water for further lyophilization of the mix at the same conditions mentioned above to obtain the physical mixture called TiO_2 + FLG 0.5 %-mortar.

2.2. Characterization techniques

XRD data were recorded on a Philips (Panalytical) model ŕXPert MPD diffractometer using Cu KAlpha1 (0.154056 nm) at 40 kV and 40 mA. Diffraction patterns were collected over a range of 5–60° 2θ at a scan rate of $0.01^\circ\ 2\theta min^{-1}$ and a scan velocity of $0.004^\circ s^{-1}$. The crystallite size, *d*, was calculated according to the Scherrer equation:

$$\boldsymbol{d} = \frac{0.9 \bullet \lambda}{2B \bullet cos\theta}$$

where B is the corrected peak width, λ = 0.154 nm, and Î¸ is the

reflection angle, in this case, the plane (1 0 1) of anatase was used.[44]

Raman spectra were recorded on an InVia Renishaw microspectrometer equipped with a 532 nm point-based laser. In all cases, power density was kept below 1 mW μm^{-2} to avoid laser heating effects. Raman analyses were performed in the solid-state under ambient conditions. The resulting spectra (after at least 30–40 random locations on each sample) were fitted with Lorentzian-shaped bands in their D, G, and 2D peaks to ascertain band positions, widths, and intensities.

UV–Vis diffuse reflectance spectra of the powder photocatalysts were registered in a Cary 5000 Agilent spectrometer equipped with an integrating sphere (using Spectralon® PTFE as internal reference).

Thermogravimetric analyses (TGA) were performed with a TGA Q50 (TA Instruments) at 10 °C min^{-1} under nitrogen flow, from 100 °C to 800 °C.

The energy of the nanocomposite band gap was determined by Tauc plots of Kubelck-Munk function from UV–Vis Diffuse Reflectance spectroscopy data,[45] considering an indirect allowed transition. [46]

Transmission Electron Microscopy (TEM) analyses were performed on stable dispersions of graphene (the same used for Raman analysis) diluted as necessary and dip-casted on Lacey copper grids (3.00 mm, 200 mesh), coated with carbon film and dried under vacuum. The samples were investigated using a High-Resolution Transmission Electron Microscope (HRTEM) JEOL 2100 at an accelerating voltage of 100 kV.

Scanning Electron Microscopy (SEM) images, elemental mapping and EDX analyses were performed in a GeminiSEM 500 field emission instrument (Zeiss). SEM images were acquired on the same lacey copper grids used in TEM analyses. Meanwhile, EDX analyses and elemental mapping were measured in pellets of the different nanocomposites. These pellets were made compressing each nanomaterial until obtaining a flat dense surface to analyze. EDX relationship where calculate dividing the percentage of C and O between the quantity obtained of Ti, only these three elements were presented in the samples.

XPS was registered with a K-Alpha Thermo Scientific spectrometer in order to obtain qualitative information about surface composition and atomic oxidation state. EDX with Microanalysis of Energy Dispersive Spectroscopy (EDS) and Electron Backscatter Diffraction (EBSD) (both of them OXFORD with advanced packages) were employed to know quantitatively the surface composition, respectively; afterwards, the corresponding XPS and EDX atomic ratios were calculated.

2.3. Photocatalytic activity

Photocatalytic runs were carried out in a semi-continuous slurry type photoreactor, previously described, [47] surrounded by 10 fluorescent lamps: 6 UV lamps (Narva LT 15 W/073 Black-Light Blue, λmax = 366 nm) and 4 Vis lamps (Narva LT 15 W/865 Cool Day-Light, λ = 400–780 nm) with a total irradiance of 40 W·m^{-2} (measured with a Kipp & Zonen model CUV-4 broadband UV radiometer; 306–383 nm).

The mixture of pesticides consisted of: $[isoproturon]_0 = [alachlor]_0 = [methomyl]_0 = [pyrimethanil]_0 = 5.0$ mg·L^{-1}. The solution containing the mixture of these pollutants at natural pH, was premixed with 200 mg L^{-1} of each photocatalyst, in dark conditions, for 30 min to guarantee homogeneous mixing in the photoreactor as well as the adsorption equilibrium of the pollutants on the photocatalysts. After that, photocatalytic runs (using 75 N cm^3 min^{-1} of oxygen flow) started by turning on all the lamps, and samples were withdrawn at selected periods to follow the reaction.

Azura Plus, Knauer High-Pressure Liquid Chromatography, HPLC, with Diode-Array detection was used to identify and quantify the pesticides after filtration of samples with 0.22 μm size hydrophilic PTFE filters. Calibration curves for each pesticide was previously constructed in identical analytical conditions within the analysis range. An Ultrasep ES PEST 5 μm (Dr. Maisch) column (250 × 3 mm) was used as stationary phase. The mobile phase was composed by ACN/acidic water (0.1 % phosphoric acid) in gradient mode, at 0.8 mL min^{-1} flow rate.

Short-chain organic acids and inorganic ions were also analyzed by an ion chromatograph with chemical suppression (Metrohm 883 Basic IC Plus) and a conductivity detector using a Metrosep A supp 7 column (250 mm length, 4 mm diameter) as stationary phase for anions and Metrosep C 6 in the case of cations; 3.6 mmol/L sodium carbonate and 1,7 mmol·L^{-1} nitric acid/1,7 mmol·L^{-1} dipicolinic acid, were the mobile phases, respectively. The total organic carbon content was determined in an infrared-detector TOC-VCSH/CSN Shimadzu analyzer.

3. Results and discussion

The synthesized TiO_2-FLG hybrid nanocomposites have been characterized by different physico-chemical techniques such as XRD, SEM, TGA, HRTEM, Raman and UV–Vis spectroscopy, to determinate their main properties, analyzing the interactions between TiO_2 nanoparticles and FLG. The XRD patterns (see Figure S.1) revealed that all these nanocomposites presented the same crystal structure, with anatase as the main crystalline phase (~97.5 %) and brookite as secondary phase (~2.5 %). Similar anatase and brookite sizes were observed when FLG was introduced into the hybrid nanocomposite, with mean crystallite sizes close to 5 nm (see Table S.1). The formation of brookite can be the consequence of a dissolution–precipitation mechanism during the synthesis of nanoparticles. The crystal structures can change due to the reactivity of the coordinated titanium complexes [48]. However, a minority proportion of brookite was always obtained in the synthesis of titania nanoparticles by the described procedure. Regarding electronic properties, almost no differences were observed when the FLG content was increased (3.07–3.14 eV, see **Table S.1**).

On the other hand, from Raman Spectroscopy (see Fig. 1 **and Table S.2**) anatase phase exhibited four Raman active modes: two E_g (151 and 633 cm^{-1}), one B_{1g} (409 cm^{-1}), and one A_{1g} (515 cm^{-1}),[49] where the peak position and broadening of the low-wavenumber E_g mode in anatase nanocrystals have commonly been explained through factors such as phonon confinement, thermal effects, and crystal defects. [50,51] These Raman active modes are showed in Fig. 1**a** for all the FLG-TiO_2 hybrid nanocomposites together with the D, G, and 2D bands from graphene that were revealed at ~ 1350 cm^{-1}, ~ 1580 cm^{-1}, and 2700 cm^{-1}. The D band (sp^3 bonds) is due to the disorder or defects in the graphene structure and G band (sp^2 bonds) arises from the stretching of the C-C bond in graphene. Meanwhile, the 2D band is interrelated to the band structure of graphene layers.[52] All the different parameters are showed in **Table S.2**. The ratio between D and G band are 0.46, 1.34, 1.08, 0.84, 0.51 for FLG, TiO_2-FLG 0.10%, TiO_2-FLG 0.25%, TiO_2-FLG 0.50% and TiO_2-FLG 1.0%, respectively. This increment is due to the defects in graphene layers by the anchorage of TiO_2 nanoparticles in their structure.

Although no significant changes have been observed by XRD, interesting differences were observed by Raman. The E_g mode (see Fig. 1**b**) was the most intense band of anatase and is commonly used for analysis [53]. The asymmetric and broadening shape of the E_g modes was evident for TiO_2-FLG 0.0%, TiO_2-FLG 0.1% and TiO_2-FLG 0.25%, which can be contributed to a phonon-confinement due to small grain sizes [54]. Whereas TiO_2-FLG 0.5% and TiO_2-FLG 1.0% showed larger and more symmetric peaks indicative of higher crystalline domains, principally in the TiO_2-FLG 0.5% nanocomposite. In general, all these hybrid photocatalysts have shown a blue shift in E_g and B_{1g} the bands (151 cm^{-1} and 409 cm^{-1}), in comparison with the TiO_2-FLG 0.0% and a red shift in the G band of graphene.

TiO_2-FLG 0.50% hybrid nanocomposite showed the lowest shift change in the E_g and B_{1g}, which is in agreement with a larger crystalline domain and the higher shift in the G band, being able to associate to hole doping in the nanocomposite.[55] There is a correlation between the intensity of the D, G and 2D band and the concentration of FLG in all the different hybrid nanocomposites. Moreover, it was possible to observe a slight shift in the 2D and G peaks from 5 to 8 cm^{-1} for all the different nanocomposites, which implies an interaction between the graphene structure and the TiO_2 nanoparticles. So, a direct correlation between

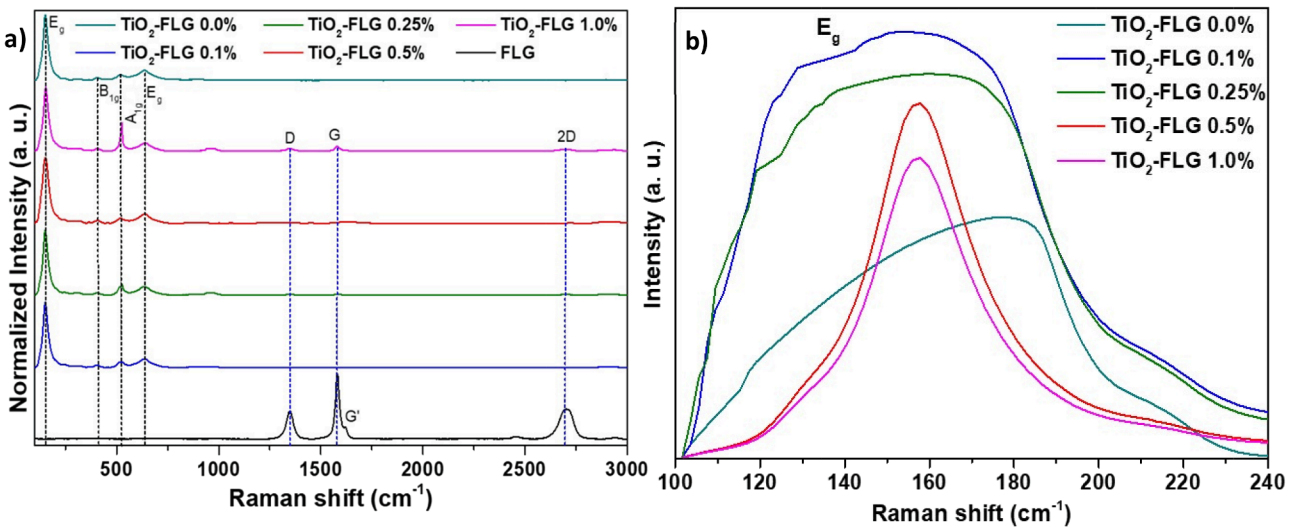

Fig. 1. Raman spectroscopy of a) the TiO_2-FLG hybrid nanocomposites and b) the E_g band of TiO_2-FLG hybrid nanocomposites.

the quantity of FLG in the nanocomposites and the relation between the intensity of the E_g from TiO_2 nanoparticle at 639 cm^{-1} and the intensity of 2D band of FLG at 2700 cm^{-1} was evidenced, which decreases with the amount of graphene. TGA analysis in air atmosphere (see **Figure S.2 and Table S.3**) was employed to characterize the thermal stability of these hybrid nanocomposites. It was possible to observe weight losses in the range between 200 and 350 °C, for as-synthesized TiO_2 nanoparticles and for all the different hybrid nanocomposites. These weight losses below 200 °C corresponded to the removal of physically adsorbed water, meanwhile, those above 200 °C corresponded to loss of surface —OH groups in the form of water and production of new Ti—O—Ti bonds [56]. Regarding the weight loss mass after 800 °C, it is possible to observe a correlation between the percentage of FLG and the percentage of loss mass at this temperature. These similar results were observed in the TGA analysis in a nitrogen atmosphere. A high thermal stability was observed under these conditions due not only to the stability of TiO_2 nanoparticles but also to the stability of FLG which did not present oxidative defects (see **Figure S.3 and Table S.4**).

Atomic composition obtained from XPS and EDX, in %, and the corresponding O/Ti atomic ratios are shown in Table 1. The data obtained from XPS are distorted by the high contamination in carbon compounds found on the surface of the photocatalysts particles, so it was not possible to draw reliable conclusions from these results. However, the results obtained from EDX followed a logical progression. As the amount of FLG increased, the proportion of titanium and oxygen decreased, and the proportion of carbon increased.

The proportion of carbon is high, if the amount added in the synthesis is considered, which indicated that FLG is mainly deposited on the surface of the TiO_2 nanoparticles, and the preparation method does not seem to be relevant in terms of composition. Finally, from a comparative analysis of O/Ti atomic ratios obtained from EDX and XPS, respectively, it can be observed that both O/Ti ratios were not dependent on FLG loading in these hybrid nanocomposites and it must be linked to TiO_2 fraction. Due to the almost no functional groups in graphene, there are no strong interactions between this nanomaterial and TiO2. Van der Waals forces, producing weak but numerous interactions mainly due to the polarity of TiO2 inducing dipoles in the p-electron cloud of graphene, may be responsible of the interactions.

The Ti 2p spectrum showed two peaks at approximately 458.8 eV (Ti 2p3/2) and 464.4 eV (Ti 2p1/2), which are typical of TiO_2 (see Figures S.4). The O 1 s spectrum also showed two peaks. The one with highest intensity was near 530 eV which is typical of metal oxides, so it can be assigned to TiO_2. The second, approximately at 531.5 eV is due to oxygenated organic functional groups. It was not possible to discern whether they belong to FLG molecules that may have been oxidized or to the contamination of organic compounds that were mentioned above.

However, although C 1 s spectrum resulted difficult to interpret because of the high carbon surface contamination, it was possible to observe in the deconvolution of this peak that a component appeared at energies close to 284 eV that was not observed in the sample without FLG. Results of deconvolution are shown in Table 2.

*B. E. (Binding Energy)

The intensities of peaks 2, 3 and 4 varied somewhat randomly, so they can be assigned to light, medium or heavily oxidized structures of the contaminating organic matter, respectively. However, peak 1 intensity increased, in general, with the amount of FLG added, from practically 0 to 9.67 %. The low value of the bonding energy also makes it possible to state that this component is due to the presence of graphene. XPS C1s deconvolution peaks of TiO_2-FLG 0.0%, TiO_2-FLG 0.5% and TiO_2-FLG 1.0% nanocomposites, respectively, were shown in **Figure S.5**, where it can be seen that, with a very tight deconvolution, in the nanocomposite containing only TiO_2 there is hardly any component of peak 1.

HRTEM and SEM images (see Fig. 2) showed the uniform distribution

Table 1
Atomic composition and O/Ti ratios of TiO_2-FLG hybrid nanocomposites and TiO_2 + FLG 0.5 % physical mixtures, respectively measured by XPS and EDX.

Nanocomposites	XPS (%)			EDX (%)			$(O/Ti)_{ratios}$	
	Ti	O	C	Ti	O	C	EDX	XPS
TiO_2-FLG 0.0 %	22.00	54.21	23.79	32.33	67.67	0.00	0.70	0.82
TiO_2-FLG 0.10 %	19.83	54.77	25.40	30.24	64.76	5.00	0.72	0.92
TiO_2-FLG 0.25 %	20.93	55.47	23.61	30.22	64.14	5.63	0.71	0.89
TiO_2-FLG 0.50 %	20.93	55.47	23.61	29.56	64.04	6.40	0.72	0.89
TiO_2-FLG 1.0 %	21.84	55.17	22.99	29.67	62.37	7.96	0.70	0.84
TiO_2 + FLG 0.5 % - Mortar	20.37	52.75	26.88	30.30	63.25	6.45	0.70	0.87
TiO_2 + FLG 0.5 % - Sonicated	20.46	54.44	25.10	28.41	65.68	5.92	0.77	0.89

Table 2
Deconvolution of C 1 s XPS spectra.

Nanocomposites	Peak 1		Peak 2		Peak 3		Peak 4	
	B. E.(eV)	%	B. E. (eV)	%	B. E. (eV)	%	B. E. (eV)	%
TiO_2-FLG 0.0 %	283.98	0.23	285.36	70.11	286.68	21.48	289.21	8.18
TiO_2-FLG 0.10 %	284.56	6.36	285.69	64.52	286.88	23.09	289.64	6.04
TiO_2-FLG 0.25 %	284.66	6.70	285.61	66.96	286.84	20.04	289.52	6.30
TiO_2-FLG 0.50 %	284.55	7.85	285.64	70.45	286.59	16.32	289.57	5.38
TiO_2-FLG 1.0 %	284.57	9.67	285.68	62.48	286.94	20.15	289.56	7.70
TiO_2 + FLG 0.5 % - Mortar	284.49	12.01	285.59	67.19	286.60	15.94	289.55	4.86
TiO_2 + FLG 0.5 % - Sonicated	284.37	6.43	285.60	84.27	286.94	6.77	289.45	2.52

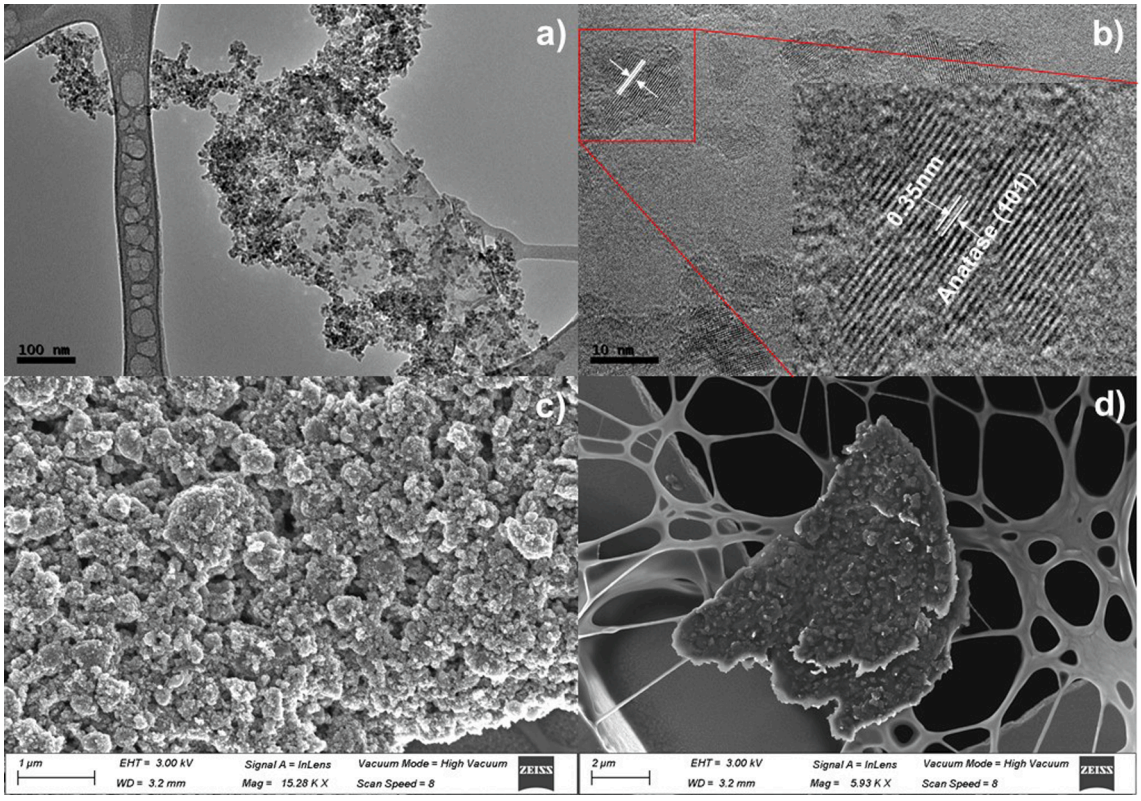

Fig. 2. Representative images of TiO_2-FLG 0.5 % hybrid nanocomposite.

of the TiO_2 nanoparticles on the sample and the crystalline phase of anatase corresponding with the plane (1 0 1) (see **Figure S.1**). The distribution size of the most representative nanocomposite TiO_2-FLG 0.5 % was showed in the **Figure S.6** with an average diameter of 9.2 ± 5.1 nm of TiO_2 nanoparticles.

The distribution of FLG on the different nanocomposites was analyzed using elemental mapping (see **Figures S.7** showing same areas analyzed by EDX in Table 1); C, Ti, and O are the elements found in the nanocomposite mapping. The proportion of titanium is very similar in all nanocomposites, with a slight increment in the carbon presence at 0.25, 0.5 and 1%.

A comparative study of the photodegradation of a selected mixture of pesticides was carried out to select the optimal FLG content in the TiO_2-FLG hybrid nanocomposite, where low concentrations of graphene were mainly used in aqueous photocatalytic applications.[57]

Photolysis runs were performance in absence of photocatalysts, and blank runs were also carried out in dark conditions under the same operating conditions. Negligible degradation was observed in any case (pesticides conversions < 5% and TOC conversions < 1%). On the other hand, adsorption equilibrium was always arisen during dark conditions, given the low FLG contents in the nanocomposite, where even lower pesticides and TOC adsorption conversions were found (<1%) in all cases.

TiO_2-FLG nanocomposites were investigated in the photocatalytic degradation of the pesticides mix. Fig. 3 **and** Table 3 show the effect of FLG loading on TOC conversions. It can be observed that the photooxidation of pesticides was improved with loading as low as 0.1 wt% of FLG (TiO_2-FLG 0.1%). However, the higher pesticides and TOC conversions were obtained by increasing the FLG content up to 0.5 wt% (TiO_2-FLG 0.5%). Though, with a higher FLG content, such as 1 wt% (TiO_2-FLG 1.0%), lower pesticides and TOC conversions were obtained, probably as a consequence of the poor radiation rate reaching titania nanoparticles, as prior deduced from XPS analysis FLG seems to wrap titania nanoparticles.

Although almost all the pesticides were removed after 300 min of irradiation time, a TOC concentration was still found at the end of the process, as it can be seen in the evolution of pesticides and TOC for all the studied TiO_2-FLG hybrid nanocomposites (see Fig. 4). Whereas complete removal of isoproturon, alachlor, and pyrimethanil were always achieved, small traces of methomyl together with some amounts of oxidation by-products remained after 5 h reaction as it was revealed by the TOC evolution curves. These oxidation products mostly

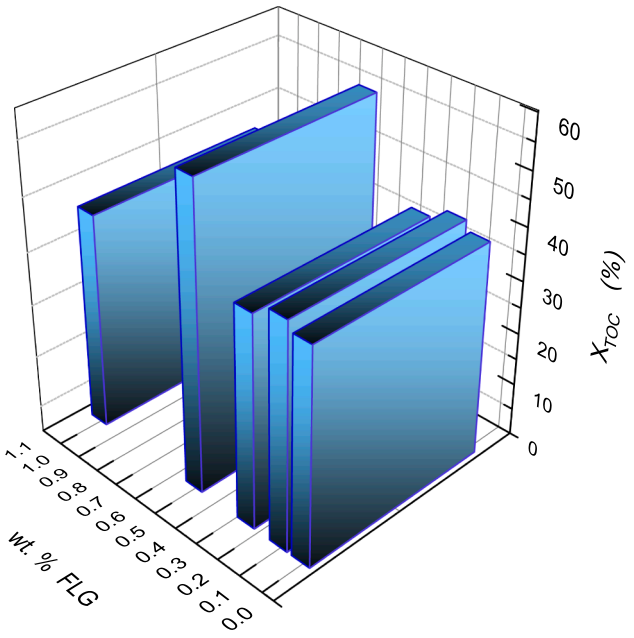

Fig. 3. Effect of percentage of FLG on photocatalytic performance at 300 min of irradiation time with the TiO_2-FLG hybrid nanocomposites.

Table 3
Pesticides and TOC conversions after 300 min of irradiation time of TiO_2-FLG nanocomposites and TiO_2 + FLG 0.5 % physical mixtures.

Nanocomposites	(%)				
	$X_{Isoproturon}$	$X_{Alachlor}$	$X_{Methomyl}$	$X_{Pyrimethanil}$	X_{TOC}
TiO_2-FLG 0.0 %	99.7 ± 0.1	93.8 ± 0.4	74.8 ± 0.2	96.4 ± 0.1	40.9 ± 0.3
TiO_2-FLG 0.10 %	94.1 ± 0.3	87.6 ± 0.3	74.1 ± 0.4	98.0 ± 0.2	42.4 ± 0.1
TiO_2-FLG 0.25 %	98.1 ± 0.4	98.7 ± 0.3	82.6 ± 0.3	100	40.8 ± 0.2
TiO_2-FLG 0.50 %	99.9 ± 0.1	98.2 ± 0.2	88.8 ± 0.1	100	57.5 ± 0.1
TiO_2-FLG 1.0 %	91.7 ± 0.2	96.3 ± 0.3	85.8 ± 0.2	97.9 ± 0.3	40.6 ± 0.4
TiO_2 + FLG 0.50 % - Mortar	87.7 ± 0.3	85.9 ± 0.2	65.8 ± 0.3	90.6 ± 0.3	36.9 ± 0.4
TiO_2 + FLG 0.50 % - Sonicated	91.4 ± 0.2	88.8 ± 0.1	76.0 ± 0.4	94.8 ± 0.1	46.7 ± 0.1

corresponded to some organic by-products and short-organic acids, mainly acetic and formic, responsible for the detected residual organic matter. In all cases, different photodegradation rates were observed for every pesticide in each titania-graphene hybrid nanocomposite, where methomyl has always presented the slowest photodegradation rate.

Most authors agree that the rate of photo-oxidation of organic pollutants with irradiated TiO_2 based photocatalysts roughly follows the Langmuir-Hinshelwood (L-H) law,[13,58] being also accepted that the corresponding rate constants and orders are only "apparent".[59]

For that reason, overall reaction rate constants are very difficult to calculate since the photocatalytic reactions are not expected to follow a simple kinetic model. The complexity of the results arises because TOC is a sum parameter, often including several by-products, that undergo manifold reactions since hydroxyl radicals react non-selectively, and numerous organic intermediates can be generated along the photocatalytic degradation frequently defined as sequential decarboxylation reaction before achieving complete mineralization to CO_2 and H_2O [60]. Therefore, considering that the photodegradation of the mixture could be suitably fitted to a modified Langmuir-Hinshelwood (L-H) kinetic scheme,[61] the apparent first order-constants values were calculated for each pesticide and shown in Fig. 5**.** In addition, the zero order TOC constants (k_{TOC}) were reckoned and reported too, for all TiO_2-FLG hybrid nanocomposites. In all cases, very good fitting parameters (r^2, with values around 0.999–0.973) were always obtained, demonstrating that the assumed kinetic model could well describe pesticides and TOC removal as pseudo-first order.

The lowest apparent kinetic constants were always found in the case of hybrid nanocomposite with the highest FLG content (TiO_2-FLG 1.0 wt %), whereas better pseudo-first-order kinetic constants were always observed when FLG content increased up to 0.5 wt%. Again, the best photodegradation pesticide constants have been achieved with TiO_2-FLG 0.5 wt%. Same performance evolution was observed in all TiO_2-FLG hybrid nanocomposites respect to the calculated zero order TOC constants (k_{TOC}), where TiO_2-FLG 0.5 % hybrid nanocomposite exhibited the higher k_{TOC} value as well.

Then, the maximum photoactivity, both in pesticides and TOC conversions at the end of irradiated reaction (300 min), was obtained with the 0.5 % wt. FLG loaded nanocomposite. This good behavior may be explained by the pairing synergy balanced between 0.5 %FLG and TiO_2, where probably the role played by FLG improved charge separation, driving to long-lasting charges which enhance the final photoefficiency. [46,62] Therefore, results indicate 0.5 wt% FLG is the optimal loading in these titania-graphene nanocomposites.

In order to understand the synergic effect between FLG and TiO_2 nanoparticles in the optimal hybrid nanocomposite, two TiO_2 + FLG physical mixtures with 0.5 wt% FLG were prepared by mixing with the corresponding TiO_2 nanoparticles, using mortar and sonication methodologies, TiO_2 + FLG 0.5% (mortar) and TiO_2 + FLG 0.5% (sonicated), respectively, for comparative purpose. The characterization of these two samples is showed in **Figures S.8–S.110**. XRD revealed the same crystallinity of the previous hybrid nanocomposites, with anatase as main crystalline phase and brookite as secondary phase (see **Figure S.8**). Raman spectroscopy (**Figure S.9a**) showed the same active modes of anatase E_g (151 and 633 cm^{-1}), one B_{1g} (409 cm^{-1}), and one A_{1g} (515 cm^{-1}), and the D, G and 2D band presented in the FLG. In **Figure S.9b** is possible to observe the highest intensity symmetric E_g band in the nanocomposite TiO_2-FLG 0.5%, followed by TiO_2 + FLG 0.5% mortar and TiO_2 + FLG 0.5% sonicated, which implies a higher crystalline domain size in the hybrid nanocomposite TiO_2-FLG 0.5%. Finally, EDX mapping (**Figure S.10**) of these two-physical mixed photocatalysts has revealed a similar correlation between the quantity of Ti and C in these mixed photocatalyst and the hybrid nanocomposites prepared by ball milling. Despite, some higher aggregates size of FLG were observed.

The evolution of pesticides concentration and TOC is shown in **Figures S.11** for these two TiO_2 + FLG 0.5% (mortar and sonicated) physical mixed photocatalysts. In both cases, pesticides and TOC conversion rates impressively slowed down (also see Table 3), demonstrating the lower photo-efficacy of these two-physical mixed photocatalysts with respect to TiO_2-FLG 0.5 % hybrid nanocomposite. It should be noted the lower pesticides and TOC conversions were always found in the photocatalyst prepared from mortar mixing, even lower than those of the hybrid nanocomposite without FLG, TiO_2-FLG 0.0%. The higher band-gap value (see **Table S.1**), could contribute to mismanage the photon flux leading to fewer photogenerated charges.

Moreover**,** it can be also emphasized the very low $k_{pesticides}$ and k_{TOC}, obtained with both physical mixed photocatalysts, especially in the case of mortar mixing photocatalyst, (see Table 4).

The long term photodegradation efficacy experiment run-up for 9 h was performed with the optimal hybrid photocatalyst, TiO_2-FLG 0.5 % (Fig. 6). Where it can be seen all the studied pesticides were completely

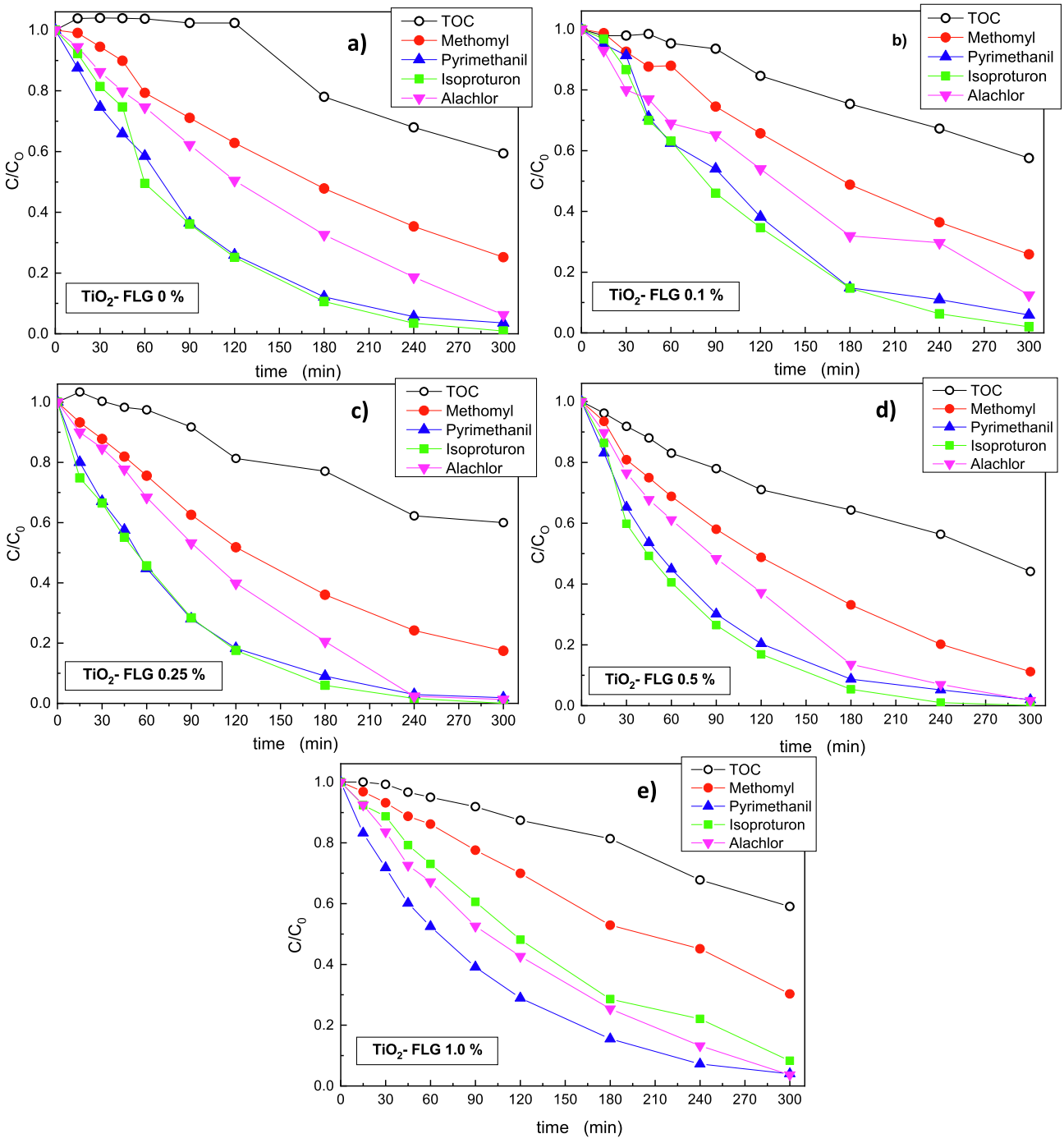

Fig. 4. Evolution of pesticides and TOC along the photocatalytic degradation with the TiO_2 - FLG 0 %, 0.1 %,0.25 %, 0.5% and 1.0% nanocomposites.

removed at 350 min of irradiation time, and around 82 % of TOC conversion was achieved at 540 min of irradiation time. Moreover, three different trends can be distinguished in TOC evolution along the photodegradation process. First, TOC evolution showed a steep slope until 350 min, where all pesticides were completely removed. Then, TOC halted between 350 and 470 min probably due to the presence of different refractory organic by-products generated during photocatalytic oxidation process, responsible of the organic matter still present in the reaction medium. And finally, TOC reduction was again addressed to reach remarkable 82% TOC removal.

On the other side, only two short-organic acids were detected, acetic and formic acid, as it can be seen in Fig. 6**B**, as final by-products before complete mineralization were achieved, together with some small concentrations of nitrate, chlorine, and higher amounts of sulfate anions, generated from the photocatalytic breakdown of these pesticides.

Finally, delving into the comprehension of the synergistic behavior between FLG and TiO_2 nanoparticles in the hybrid photocatalysts, the role of surface graphitic carbon in the TOC conversion was studied. In Fig. 7, C data calculated from C-XPS percentage (Table 1) and C-XPS deconvolution peak percentage at around 283.9 eV (Table 2), has been graphed *vs*. the corresponding TOC conversions at 300 min of irradiation time. A percentage of graphitic carbon in surface around 1.9 % in the TiO_2-FLG 0.5% hybrid nanocomposite has led to the best photoefficiency in the degradation of the pesticides studied here. Moreover, worst TOC values were arisen when C amount on the photocatalyst surface was increased, emphasizing the lowest TOC removal found in

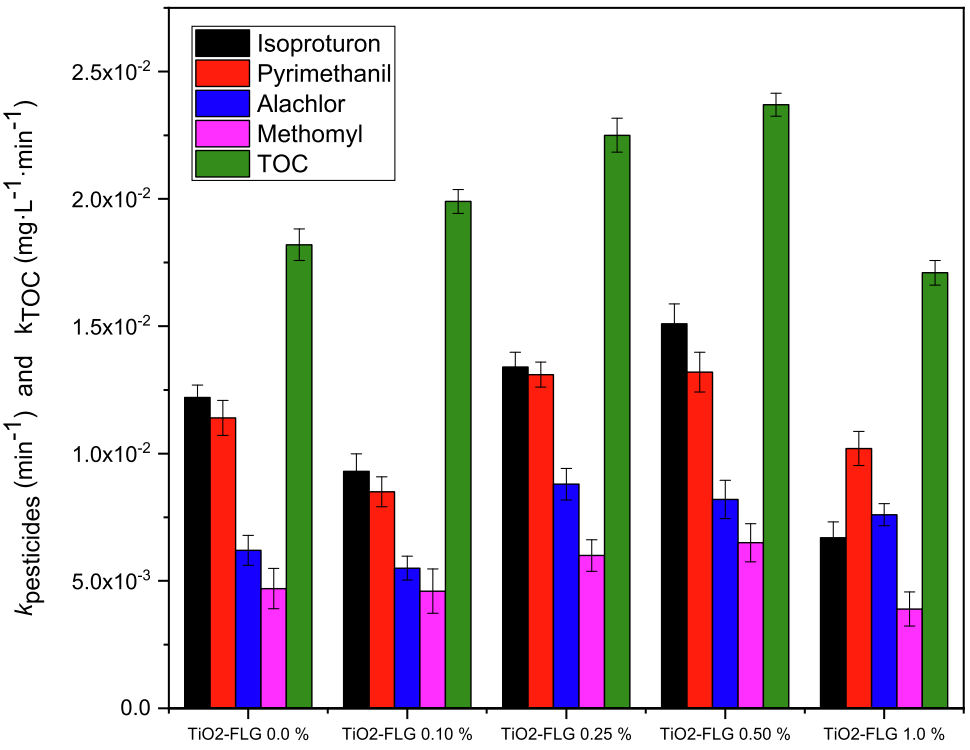

Fig. 5. Effect of FLG loading on pesticides and TOC apparent kinetic constants for all TiO_2-FLG hybrid nanocomposites.

Table 4
Pseudo-first kinetic constants of pesticides and TOC pseudo- kinetic constants for TiO_2 + FLG 0.50 % mixed photocatalysts and TiO_2-FLG 0.50 % hybrid nanocomposite.

Nanocomposites	Pesticide								TOC	
	$k_{Isoproturon}$ (min^{-1})	r^2	$k_{Pyrimethanil}$ (min^{-1})	r^2	$k_{Alachlor}$ (min^{-1})	r^2	$k_{Methomyl}$ (min^{-1})	r^2	k_{TOC} ($mg{\cdot}L^{-1}{\cdot}min^{-1}$)	r^2
TiO_2 + FLG 0.50 % - Mortar	0.0049	0.942	0.0074	0.966	0.0063	0.917	0.0035	0.998	0.0146	0.993
TiO_2 + FLG 0.50 % - Sonicated	0.0059	0.946	0.0076	0.941	0.0041	0.994	0.0046	0.987	0.0197	0.991
TiO_2-FLG 0.50 % Hybrid nanocomposite	0.0151	0.990	0.0132	0.999	0.0082	0.998	0.0065	0.995	0.0237	0.995

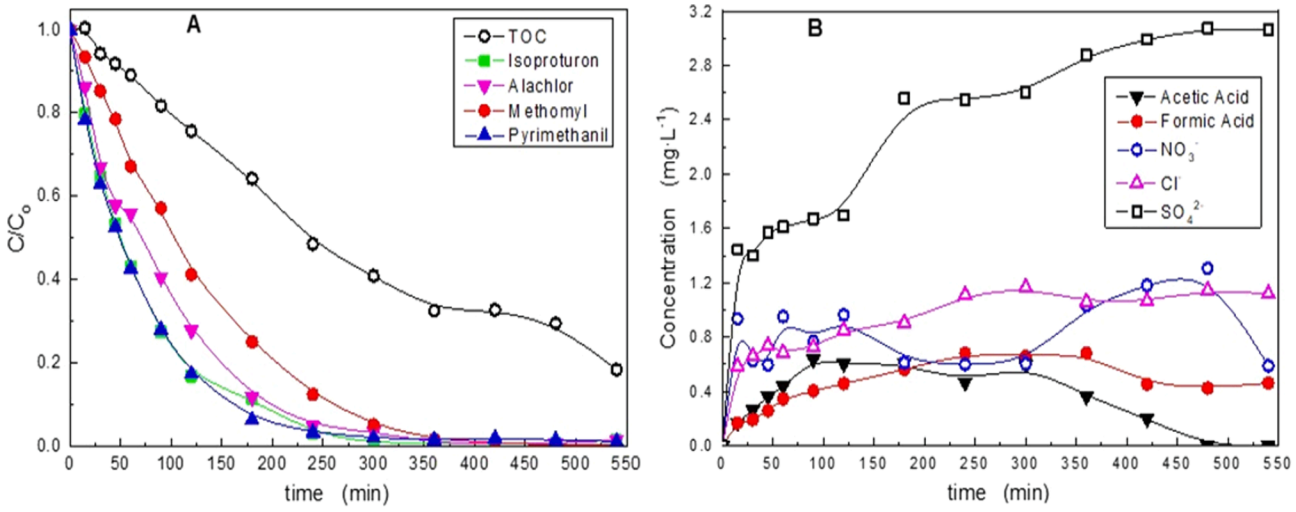

Fig. 6. Photodegradation of the selected mixture of pesticides with the TiO_2-FLG 0.5 % hybrid nanocomposite at 550 min of irradiation time: (A) Evolution of pesticides and TOC; and (B) Evolution of aromatic intermediates, sulfates, nitrates, and chlorine anions from the photocatalytic degradation of pesticides.

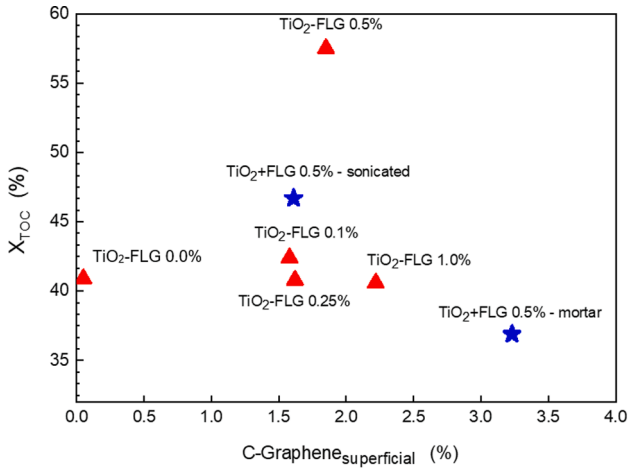

Fig. 7. Effect of graphitic carbon in surface (%) on TOC conversions at 300 min of irradiation time (▲TiO_2-FLG hybrid nanocomposites; ⋆TiO_2 + FLG 0.5% physical mixtures).

the case of TiO_2 + FLG 0.5 % - mortar photocatalyst.

Therefore, from the obtained results can be assumed that the junction between titania nanoparticles and FLG is more efficient in the case of hybrid nanocomposites than in the case of physical mixtures, even at the optimal FLG loading, where a detrimental effect on the pesticides photodegradation was always observed respect to the TiO_2-FLG 0.5 % hybrid nanocomposite.

4. Conclusions

A mechanochemical treatment has been proposed as new ecofriendly methodology to synthesize green titania-graphene nanocomposites for their application in the photocatalytic degradation of a complex mixing of pesticides, classified by EU as priority pollutants (isoproturon, pyrimethanil, alachlor and methomyl).

From XRD patterns all these photocatalysts have presented the same crystal structure with anatase as the main crystalline phase (≈ 97.5 %) and brookite as secondary phase (≈ 2.5 %).

It can be concluded from EDX and XPS analysis that as the amount of FLG increased, the proportion of titanium and oxygen decreased and the proportion of carbon increased, which indicates that FLG is mainly deposited on the surface of the TiO_2 nanoparticles, wrapping them. Moreover, an interaction between the graphene structure and the TiO_2 nanoparticles can be assumed by Raman spectra results, where it is possible to observe a slight shift in the 2D and G peaks for all the different prepared TiO_2-FLG hybrid nanocomposites and a higher crystalline domain size for TiO_2-FLG-0.5% nanocomposite, without any further annealing step.

The best photocatalytic performance in the degradation of pesticides was obtained by TiO_2-FLG 0.5 % hybrid nanocomposite, where all the pesticides were completely removed at 350 min, and around 82 % of TOC conversion was achieved at 540 min of irradiation time.

Physical mixtures of TiO_2 nanoparticles and 0.5% FLG prepared by mortar or sonication exhibited worst photoefficiency and lower TOC conversion, leading to deduce the existence of pairing synergy balanced between 0.5 %FLG and TiO_2, ball milling prepared, where probably the role played by FLG improved charge separation, driving to long-lasting charges which enhance the final photoefficiency.

Whereas a percentage of graphitic carbon in surface around 1.9 % was obtained in the optimal TiO_2-FLG 0.5 % nanocomposite, worst TOC values were arisen when C amount on the photocatalyst surface was increased, emphasizing the lowest TOC removal found in the case of TiO_2 + FLG 0.5 % - mortar photocatalyst.

Declaration of Competing Interest

The authors declare that they have no known competing financial interests or personal relationships that could have appeared to influence the work reported in this paper.

Acknowledgements

Financial support from the EU Graphene-based disruptive technologies, Graphene Flagship core 3 (881603), the Spanish *Ministerio de Economía y Competitividad* (Projects CTQ2017-88158-R and CTQ2015-71238-R) (MINECO/FEDER), RTI2018-094958-B-I00 (MCIU/AEI/FEDER, UE), Junta *Comunidades de Castilla-La Mancha* (project SBPL4/17/180501/000204) and Junta de Extremadura/FEDER (project GRU18035) are gratefully acknowledged. Beatriz Villajos thanks the Spanish *Ministerio de Economía y Competitividad* for her AEI contract (PRE2019-089049). Raman spectra were collected using a Spectrometer confocal Renishaw InVia Reflex (FEDER-JCCM funding, UNCM13-1E-1663), included in the facilities of the Instituto Regional de Investigación Científica Aplicada (IRICA), which is also acknowledged for technical support. The authors would like to thank Eduardo Prado García Consuegra and Alicia Fraile Chamizo for their technical assistance.

Appendix A. Supplementary material

Supplementary data to this article can be found online at https://doi.org/10.1016/j.seppur.2022.120638.

References

[1] M. Syafrudin, R.A. Kristanti, A. Yuniarto, T. Hadibarata, J. Rhee, W.A. Al-onazi, T. S. Algarni, A.H. Almarri, A.M. Al-Mohaimeed, Pesticides in Drinking Water-A Review, Int J Environ Res Public Health 18 (2) (2021) 468, https://doi.org/10.3390/ijerph18020468.

[2] E. Castillejos, A. Esteban-Arranz, B. Bachiller-Baeza, I. Rodríguez-Ramos, A. Guerrero-Ruiz, Reductive degradation of 2,4-dichlorophenoxyacetic acid using Pd/carbon with bifunctional mechanism, Catal. Today 357 (2020) 361–367.

[3] S. Khalid, I. Hashmi, S.J. Khan, Bacterial assisted degradation of chlorpyrifos: The key role of environmental conditions, trace metals and organic solvents, J Environ Manage 168 (2016) 1–9.

[4] S. Ahmed, M.G. Rasul, R. Brown, M.A. Hashib, Influence of parameters on the heterogeneous photocatalytic degradation of pesticides and phenolic contaminants in wastewater: a short review, J Environ Manage 92 (3) (2011) 311–330.

[5] A.H. Keihan, R. Hosseinzadeh, M. Farhadian, H. Kooshki, G. Hosseinzadeh, Solvothermal preparation of Ag nanoparticle and graphene co-loaded TiO2 for the photocatalytic degradation of paraoxon pesticide under visible light irradiation, RSC Adv. 6 (87) (2016) 83673–83687.

[6] G.R. Echavia, F. Matzusawa, N. Negishi, Photocatalytic degradation of organophosphate and phosphonoglycine pesticides using TiO_2 immobilized on silica gel, Chemosphere 76 (2009) 595–600.

[7] N.H. Ince, I.G. Apikyan, Combination of activated carbon adsorption with light-enhanced chemical oxidation via hydrogen peroxide, Water Res. 34 (2000) 4169–4176.

[8] R. Andreozzi, Advanced oxidation processes (AOP) for water purification and recovery, Catal. Today 53 (1999) 51–59.

[9] D. Ravelli, D. Dondi, M. Fagnoni, A. Albini, Photocatalysis, A multi-faceted concept for green chemistry, Chem Soc Rev 38 (2009) 1999–2011.

[10] J. Carbajo, M. Jiménez, S. Miralles, S. Malato, M. Faraldos, A. Bahamonde, Study of application of titania catalysts on solar photocatalysis: Influence of type of pollutants and water matrices, Chem. Eng. J. 291 (2016) 64–73.

[11] G. Luna-Sanguino, A. Ruiz-Delgado, A. Tolosana-Moranchel, L. Pascual, S. Malato, A. Bahamonde, M. Faraldos, Solar photocatalytic degradation of pesticides over TiO2-rGO nanocomposites at pilot plant scale, Sci Total Environ 737 (2020), 140286.

[12] M.N. Chong, B.o. Jin, C.W.K. Chow, C. Saint, Recent developments in photocatalytic water treatment technology: a review, Water Res 44 (10) (2010) 2997–3027.

[13] S. Malato, P. Fernández-Ibáñez, M.I. Maldonado, J. Blanco, W. Gernjak, Decontamination and disinfection of water by solar photocatalysis: Recent overview and trends, Catal. Today 147 (1) (2009) 1–59.

[14] E.-H. Kong, J. Lim, J.H. Lee, W. Choi, H.M. Jang, Enhanced photocatalytic activity of {101}-oriented bipyramidal TiO2 agglomerates through interparticle charge transfer, Appl. Catal. B 176–177 (2015) 76–82.

[15] B. Tryba, Increase of the Photocatalytic Activity of by Carbon and Iron Modifications, Int. J. Photoenergy 2008 (2008) 1–15.

[16] J. Chen, F. Qiu, W. Xu, S. Cao, H. Zhu, Recent progress in enhancing photocatalytic efficiency of TiO 2 -based materials, Appl. Catal. A 495 (2015) 131–140.
[17] S. Li, Y. Yang, Q. Su, X. Liu, H. Zhao, Z. Zhao, J. Li, C. Jin, Synthesis and photocatalytic activity of transition metal and rare earth element co-doped TiO2 nano particles, Mater. Lett. 252 (2019) 123–125.
[18] Q.-F. Liu, Q. Zhang, B.-R. Liu, S. Li, J.-J. Ma, Building surface defects by doping with transition metal on ultrafine TiO2 to enhance the photocatalytic H2 production activity, Chin. J. Catal. 39 (2018) 542–548.
[19] S. Kohtani, S. Makino, A. Kudo, K. Tokumura, Y. Ishigaki, T. Matsunaga, O. Nikaido, K. Hayakawa, R. Nakagaki, Photocatalytic Degradation of 4-n-Nonylphenol under Irradiation from Solar Simulator: Comparison between BiVO4and TiO2Photocatalysts, Chem. Lett. 31 (2002) 660–661.
[20] A. Nourbakhsh, S. Abbaspour, M. Masood, S.N. Mirsattari, A. Vahedi, K.J. D. Mackenzie, Photocatalytic properties of mesoporous TiO2 nanocomposites modified with carbon nanotubes and copper, Ceram. Int. 42 (2016) 11901–11906.
[21] M. Cruz, C. Gomez, C.J. Duran-Valle, L.M. Pastrana-Martínez, J.L. Faria, A.M. T. Silva, M. Faraldos, A. Bahamonde, Bare TiO 2 and graphene oxide TiO 2 photocatalysts on the degradation of selected pesticides and influence of the water matrix, Appl. Surf. Sci. 416 (2017) 1013–1021.
[22] L. Lin, H. Wang, P. Xu, Immobilized TiO2-reduced graphene oxide nanocomposites on optical fibers as high performance photocatalysts for degradation of pharmaceuticals, Chem. Eng. J. 310 (2017) 389–398.
[23] R. Spitz Steinberg, M. Cruz, N.G.A. Mahfouz, Y. Qiu, R.H. Hurt, Breathable Vapor Toxicant Barriers Based on Multilayer Graphene Oxide 11 (2017) 5670–5679.
[24] R.A. Doong, C.Y. Liao, Enhanced visible-light-responsive photodegradation of bisphenol A by Cu, N-codoped titanate nanotubes prepared by microwave-assisted hydrothermal method, J Hazard Mater 322 (2017) 254–262.
[25] X. He, W.G. Aker, M. Pelaez, Y. Lin, D.D. Dionysiou, H.-M. Hwang, Assessment of nitrogen–fluorine-codoped TiO2 under visible light for degradation of BPA: Implication for field remediation, J. Photochem. Photobiol., A 314 (2016) 81–92.
[26] C. Chen, Y. Zhang, J. Zeng, F. Zhang, K. Zhou, C.R. Bowen, D. Zhang, Aligned macroporous TiO2/chitosan/reduced graphene oxide (rGO) composites for photocatalytic applications, Appl. Surf. Sci. 424 (2017) 170–176.
[27] Y. Yu, J.C. Yu, C.-Y. Chan, Y.-K. Che, J.-C. Zhao, L. Ding, W.-K. Ge, P.-K. Wong, Enhancement of adsorption and photocatalytic activity of TiO2 by using carbon nanotubes for the treatment of azo dye, Appl. Catal. B 61 (2005) 1–11.
[28] A. Dhakshinamoorthy, S. Navalon, A. Corma, H. Garcia, Photocatalytic CO2 reduction by TiO2 and related titanium containing solids, Energy Environ. Sci. 5 (11) (2012) 9217, https://doi.org/10.1039/c2ee21948d.
[29] F. Lu, D. Astruc, Nanocatalysts and other nanomaterials for water remediation from organic pollutants, Coord. Chem. Rev. 408 (2020) 213180, https://doi.org/10.1016/j.ccr.2020.213180.
[30] A.K. Geim, Graphene: status and prospects, Science 324 (2009) 1530–1534.
[31] A.K. Geim, K.S. Novoselov, The rise of graphene, Nat Mater 6 (3) (2007) 183–191.
[32] B. Kuchta, L. Firlej, A. Mohammadhosseini, P. Boulet, M. Beckner, J. Romanos, P. Pfeifer, Hypothetical high-surface-area carbons with exceptional hydrogen storage capacities: open carbon frameworks, J Am Chem Soc 134 (36) (2012) 15130–15137.
[33] X. Huang, X. Qi, F. Boey, H. Zhang, Graphene-based composites, Chem Soc Rev 41 (2) (2012) 666–686.
[34] F. Zou, Y. Yu, N.a. Cao, L. Wu, J. Zhi, A novel approach for synthesis of TiO2–graphene nanocomposites and their photoelectrical properties, Scr. Mater. 64 (7) (2011) 621–624.
[35] S. Kumari, A. Shekhar, D.D. Pathak, Graphene oxide–TiO2 composite: an efficient heterogeneous catalyst for the green synthesis of pyrazoles and pyridines, New J. Chem. 40 (6) (2016) 5053–5060.
[36] Y. Liu, D. Zhang, The preparation of reduced graphene oxide-TiO 2 composite materials towards transparent, strain sensing and photodegradation multifunctional films, Compos. Sci. Technol. 137 (2016) 102–108.
[37] S. Pu, R. Zhu, H. Ma, D. Deng, X. Pei, F. Qi, W. Chu, Facile in-situ design strategy to disperse TiO2 nanoparticles on graphene for the enhanced photocatalytic degradation of rhodamine 6G, Appl. Catal. B 218 (2017) 208–219.
[38] C. Lai, M.-M. Wang, G.-M. Zeng, Y.-G. Liu, D.-L. Huang, C. Zhang, R.-Z. Wang, P. Xu, M. Cheng, C. Huang, H.-P. Wu, L. Qin, Synthesis of surface molecular imprinted TiO2/graphene photocatalyst and its highly efficient photocatalytic degradation of target pollutant under visible light irradiation, Appl. Surf. Sci. 390 (2016) 368–376.
[39] D.J. Li, Z. Huang, T.H. Hwang, R. Narayan, J.W. Choi, S.O. Kim, Atomic thin titania nanosheet-coupled reduced graphene oxide 2D heterostructures for enhanced photocatalytic activity and fast lithium storage, Electron. Mater. Lett. 12 (2016) 211–218.
[40] S.-M.-T.-L.-M. Pastrana-Martínez, A.G. Kontos, N.G. Moustakas, J.L. Faria, J. M. Doña-Rodríguez, P. Falaras, A.M.T. Silva, Nanostructured carbon–TiO2 photocatalysts for water purification: an overview, Chem. Eng. J. 224 (2013) 17–23.
[41] J.M. González-Domínguez, V. León, M.I. Lucío, M. Prato, E. Vázquez, Production of ready-to-use few-layer graphene in aqueous suspensions, Nat Protoc 13 (3) (2018) 495–506.
[42] V. León, J.M. González-Domínguez, J.L.G. Fierro, M. Prato, E. Vázquez, Production and stability of mechanochemically exfoliated graphene in water and culture media, Nanoscale 8 (30) (2016) 14548–14555.
[43] J.R. Centre (Ed.), Development of the first Watch List under the Environmental Quality Standards Directive, 2015.
[44] B.D.C.S.R. Stock, Elements Of X-ray Diffraction, 3rd ed., 2001.
[45] H.N.D.Z. Chen, E. Miller, Photoelectrochemical Water Splitting: Standards, Experimental Methods, and Protocols, Springer, 2013.
[46] A. Tolosana-Moranchel, J.A. Casas, A. Bahamonde, L. Pascual, L.I. Granone, J. Schneider, R. Dillert, D.W. Bahnemann, Nature and photoreactivity of TiO2-rGO nanocomposites in aqueous suspensions under UV-A irradiation, Appl. Catal. B 241 (2019) 375–384.
[47] P. García-Muñoz, J. Carbajo, M. Faraldos, A. Bahamonde, Photocatalytic degradation of phenol and isoproturon: Effect of adding an activated carbon to titania catalyst, J. Photochem. Photobiol., A 287 (2014) 8–18.
[48] S. Sun, P. Song, J. Cui, S. Liang, Amorphous TiO2 nanostructures: synthesis, fundamental properties and photocatalytic applications, Catalysis, Science & Technology 9 (2019) 4198–4215.
[49] W.F. Zhang, Y.L. He, M.S. Zhang, Z. Yin, Q. Chen, Raman scattering study on anatase TiO2nanocrystals, J. Phys. D Appl. Phys. 33 (2000) 912–916.
[50] K.-R. Zhu, M.-S. Zhang, Q. Chen, Z. Yin, Size and phonon-confinement effects on low-frequency Raman mode of anatase TiO2 nanocrystal, Phys. Lett. A 340 (2005) 220–227.
[51] D. Georgescu, L. Baia, O. Ersen, M. Baia, S. Simon, Experimental assessment of the phonon confinement in TiO2 anatase nanocrystallites by Raman spectroscopy, J. Raman Spectrosc. 43 (2012) 876–883.
[52] A.C. Ferrari, Raman spectroscopy of graphene and graphite: Disorder, electron–phonon coupling, doping and nonadiabatic effects, Solid State Commun. 143 (2007) 47–57.
[53] V. Swamy, A. Kuznetsov, L.S. Dubrovinsky, R.A. Caruso, D.G. Shchukin, B. C. Muddle, Finite-size and pressure effects on the Raman spectrum of nanocrystalline anataseTiO2, Physical Review B 71 (2005).
[54] S. Kelly, F.H. Pollak, M. Tomkiewicz, Raman Spectroscopy as a Morphological Probe for TiO2Aerogels, J. Phys. Chem. B 101 (1997) 2730–2734.
[55] B. Tang, H. Guoxin, H. Gao, Raman Spectroscopic Characterization of Graphene, Appl. Spectrosc. Rev. 45 (2010) 369–407.
[56] T. Bezrodna, G. Puchkovska, V. Shymanovska, J. Baran, H. Ratajczak, IR-analysis of H-bonded H2O on the pure TiO2 surface, J. Mol. Struct. 700 (2004) 175–181.
[57] M. Faraldos, A. Bahamonde, Environmental applications of titania-graphene photocatalysts, Catal. Today 285 (2017) 13–28.
[58] A. Tolosana-Moranchel, J.A. Casas, J. Carbajo, M. Faraldos, A. Bahamonde, Influence of TiO2 optical parameters in a slurry photocatalytic reactor: Kinetic modelling, Appl. Catal. B 200 (2017) 164–173.
[59] R. Scotti, M. D'Arienzo, A. Testino, F. Morazzoni, Photocatalytic mineralization of phenol catalyzed by pure and mixed phase hydrothermal titanium dioxide, Appl. Catal. B 88 (2009) 497–504.
[60] V. Augugliaro, M. Bellardita, V. Loddo, G. Palmisano, L. Palmisano, S. Yurdakal, Overview on oxidation mechanisms of organic compounds by TiO2 in heterogeneous photocatalysis, J. Photochem. Photobiology C: Photochem. Rev. 13 (3) (2012) 224–245.
[61] K.V. Kumar, K. Porkodi, F. Rocha, Langmuir-Hinshelwood kinetics – A theoretical study, Catal. Commun. 9 (1) (2008) 82–84.
[62] Á. Tolosana-Moranchel, A. Manassero, M.L. Satuf, O.M. Alfano, J.A. Casas, A. Bahamonde, Influence of TIO2-rGO optical properties on the photocatalytic activity and efficiency to photodegrade an emerging pollutant, Appl. Catalysis B: Environmental 246 (2019) 1–11.